Iron bed accelerator for discharging cylindrical NCA battery in salt solution

Erdenebold Urtnasan[1,2], Jei-Pil Wang[3*]

[1]Industrial Science Technology Research Center, Pukyong National University, Busan 48513, Republic of Korea.
[2]Darkhan School of Technology, Mongolian University of Science and Technology, Darkhan city, Mongolia.
[3]Department of Metallurgical Engineering, BB21 plus team, Pukyong National University, Busan 48513, Korea.

Corresponding author: Jei-Pil Wang (*Email: jpwang@pknu.ac.kr*)

Abstract

This study examines the iron bed accelerator for discharging cylindrical NCA batteries in salt solution. The use of Li-ion batteries has increased due to the rise of e-mobility in computers, cell phones, and electric vehicles. Recycling Li-ion batteries for raw material in lithium-ion battery production is increasingly important as the revolution unfolds. When disposing of, transporting, and recycling the battery, it is important to crush it to separate the black mass, plastic, and metal components. However, there is a potential explosion risk due to the remaining voltage in the battery. In recycling, the discharge step is significant. The research aimed to test a new method for discharging cylinder batteries using saltwater and an iron bed. Higher NaCl content increases pH and lowers electrochemical potential for water electrolysis. This unique combination enables the battery to discharge at a high rate. In 6 hours, the battery discharged in a 20 wt.% salt solution with 99.6% efficiency. The battery discharge efficiency decreased when exposed to 25 wt% and 30 wt% salt solutions, attributed to reduced water electrolysis intensity. According to the results of various experiments, it has been observed that as the temperature of the salt solution rises, there is a slight increase in the rate of battery discharge; however, no significant difference has been observed. This article talks about how batteries are discharged. It shows the electrochemical reaction using the Eh-pH diagram for Fe-Na-Cl. It also has a schematic diagram that shows the process and a chemical analysis of the precipitate that forms during the discharge test.

Keywords: Electrolyte solution, Iron bed, Positive pole, Residual voltage, Voltage drop, Discharge rate, Salt water.

Competing Interests: The authors declare that they have no competing interests.
Authors' Contributions: Performed the experiments, conducted writing, E.U.; reviewed and checked the manuscript, J.P.W. Both authors have read and agreed to the published version of the manuscript.
Transparency: The authors confirm that the manuscript is an honest, accurate, and transparent account of the study; that no vital features of the study have been omitted; and that any discrepancies from the study as planned have been explained. This study followed all ethical practices during writing.
Institutional Review Board Statement: Not applicable.

1. Introduction

In recent years, the application of Li-Ion batteries (LIBs) has seen a surge due to the rise in demand for electrical products, particularly electric vehicles. Lithium batteries come in a range of high-capacity options, depending on the metals used in the cathode [1-4]. In the field of electrical applications, the most widely used types of cylindrical lithium-ion batteries include LMO (lithium-ion manganese oxide−$LiMn_2O_4$), NMC (Nickel Manganese Cobalt−$LiNiMnCoO_2$), NCA (Lithium nickel cobalt aluminum oxides−$LiNiCoAlO_2$), LFP (lithium iron phosphate−$LiFePO_4$), and LCO (Lithium Cobalt Oxide−$LiCoO_2$) [5-8]. By highlighting the use of waste batteries as a viable raw material, battery manufacturers are able to lower the overall cost of producing batteries. Many researchers have been conducting multiple studies concurrently, with the objective of recycling LIBs and extracting valuable cathode metals like nickel and cobalt. The process of transporting, depositing, and crushing batteries for recycle is often complicated by the recurring issue of battery explosions. In the event that the batteries are not discharged, it is possible for a short circuit to occur when the anode and cathode make contact with each other as a result of external influences. This can lead to ignition and ultimately result in an explosion [9-13]. When it comes to discharging batteries before crushing, freezing, and electrolytic discharge methods are the most prevalent options that are utilized. Electric discharge is one of the methods used to load electricity into the battery. However, the reason why most recycling processes do not widely adopt it is because the process is lengthy and time-consuming. The freezing method effectively reduces battery voltages to a level that is considered safe. The vacuum and inert atmosphere, which are achieved by using shielding gases such as Ar and CO_2, effectively eliminate the potential danger of battery explosion [14-16]. Note that specialized freezing equipment is necessary when using freezing methods. Moreover, if you choose the quick-freezing method, be prepared for the additional cost of expensive nitrogen gas, resulting in higher processing costs. Additionally, when using quick-freezing technique, it is important to consider the anticipated expense of nitrogen gas, which is recognized for its high cost, leading to increased processing expenses.

When recycling lithium-ion batteries, it is important to consider the discharge that occurs in large qunatities. One possible solution to this challenge is to simultaneously discharge the batteries while immersing them in an electrolyte solution. The technique of submerging the battery in an electrolyte solution relies on a diverse range of electrochemical reactions and the manifestation of various electrolysis phenomena. The researchers, Zhang, et al. [17]; Xiao, et al. [18]; Liu, et al. [19], and Xu, et al. [20], conducted discharge experiments on LIBs using different electrolyte solutions. They compared the effects of direct immersion and connecting poles of the battery with external platinum wire in salt solutions such as NaCl, Na_2SO_4, $FeSO_4$, and $ZnSO_4$. In their experiments, Ojanen, et al. [12] and Torabian, et al. [13] tested various salt solutions, including NaCl, Na_2S, and $MgSO_4$, with concentrations ranging from 5 to 30 wt.%. They concluded that the NaCl solution was the most effective. Due to the corrosive nature of batteries when submerged in a salt solution, Ojanen, et al. [12] conducted a study with the objective of enhancing electrical conductivity. They achieved this by introducing iron powder, which contacted the battery through a platinum wire, ultimately leading to an accelerated discharge rate. Iron's standard electrode potential of -0.447V enables the formation of an active electric cell in the electrolyte solution. Iron has a high electrical resistance, leading to the rapid loss of battery voltage and the conversion of energy into heat. Additionally, Ojanen, et al. [12] found that the presence of iron powder in battery discharge improves discharge efficiency in comparison to zinc powder (E°=−0.76V). Furthermore, it's important to note that obtaining iron is both easy and affordable. Our objective was to intentionally create a short circuit in the electrical cell by introducing a salt solution between the battery and the iron components. In order to ensure that the battery discharge is spread throughout the salt solution, a significant quantity of metal is utilized to effectively conduct the electric current. Our research is notable because we prioritized finding a simple method to discharge the battery in salt water with iron parts, while avoiding any harm to the battery components and preventing corrosion. Additionally, in our study, we examined the impact of both the concentration of salt water and the temperature on the discharge rate. In order to enhance understanding of the discharge process, we have included a detailed explanation along with a schematic diagram and a Pourbaix diagram. These diagrams are specifically created to depict the areas of thermodynamic stability and the electrochemical reactions that are involved. Once the experiment concluded, we thoroughly examined the precipitate that had formed in the liquid. The analysis results confirmed the initial assumption that electrochemical reactions take place.

2. Materials and Methods

2.1. Experimental Materials

For our research, we chose to utilize Samsung cylindrical-type lithium-ion NCA (Nickel Cobalt Aluminum Oxides) batteries (with a voltage of 3.78 V) as the main experimental materials. The NCA battery, which we carefully separated from a package of 32 V set, had specific details, including a reported nominal capacity of 3950 mAh, a minimum capacity of 2850 mAh, and a nominal voltage of 3.78 V. We effectively discharge the batteries by immersing them entirely in salt water, applying a voltage of 3.78 V. In order to create the salt water, we specifically chose SAJO Company, a popular sea salt brand known for its purity and sourced from South Korea. The composition of sea salt consists of approximately 93 to 94.5% NaCl, along with a mixture of minerals including MgCl, Na_2SO_4, $MgSO_4$, KCl, and $CaSO_4$. The concentration and pH level of the salt water used during the discharge experiment are presented in Table 1, providing valuable information. When we added Sajo sea salt by weight mass ranging from 10 to 30 wt.% to 500 ml of distilled water in order to create a salt solution, we observed that the salt did not dissolve as rapidly as we had initially expected. In order to speed up the process, we took the initiative to start stirring the mixture so that it would dissolve completely. The pH level of the salt water, which had a concentration ranging from 10 to 30 wt.%, was measured using a digital pH-200 pH meter and found to be between 9.75 and 10.63. However, adding more salt led to a slight increase in the pH level. 100 grams of iron were added to the bottom of the beaker filled with the solution, in order to expedite the discharge process. The iron employed in this process was finely ground into a powder, ensuring an exceptional purity level of 99.8%.

Table 1.
The concentration and pH level of saltwater.

Concentration	Salt in water, g per 500 ml	pH
10 wt.%	5	9.75
15 wt.%	7.5	10.36
20 wt.%	10	10.49
25 wt.%	12.5	10.60
30 wt.%	15	10.63

2.2. Experimental Procedures

During the investigation of methods to enhance the rate of battery discharge in salt water using an iron bed, researchers have primarily concentrated on examining two key variables: the concentration level and temperature of the solution. Figure 1 shows a schematic representation that depicts the battery's location during the discharge test, as well as the electrical circuit involving the iron bed. During the experiment, a layer of iron powder was carefully placed at the bottom of the beaker, which already contained the solution. Next, we immersed a cylindrical battery into the iron bed, as shown in Figure 1. When the electric current passes through the iron components, it triggers an electrochemical response on the extensive surface of the iron particles, resulting in a swift reduction of the battery voltage. The process of electrochemical reactions can lead to the production and deposition of iron oxides and chlorides on the surface of iron particles. This experiment conducted the battery discharge process, involving its submersion into iron powder, in a salt solution at temperatures ranging from 25 to 65 °C. The experiment utilized a SciLab brand digital hotplate magnetic stirrer. The experiment began with setting the hot plate to a specific temperature for one hour, then placing the beaker containing salt water and iron powder on it. After this, we submerged the battery into the iron powder and started the experiment. The battery's voltages were measured on an hourly basis throughout the duration.
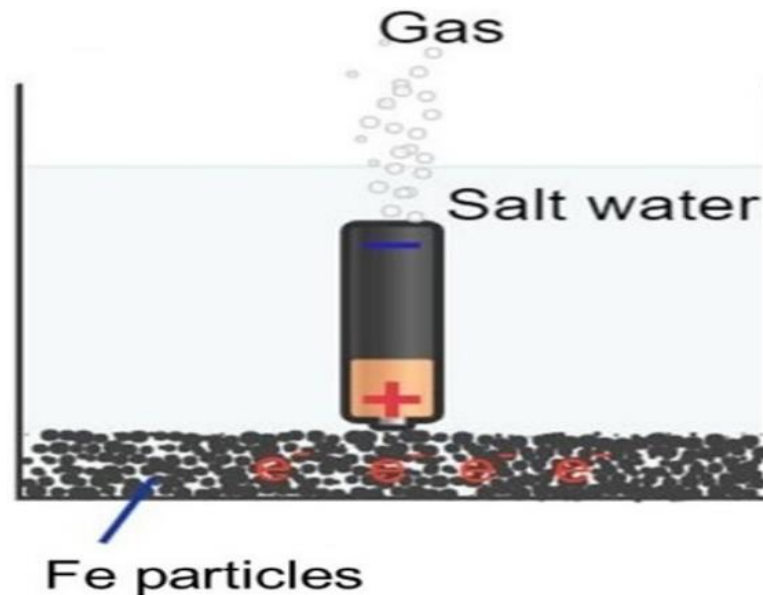
Figure 1.
Schematic diagram of electrochemical discharge using salt water with iron particle bed.

2.3. Analysis Methods

In the experiment, we used a UT201 clamp multimeter to measure the low voltage of the battery. To obtain an accurate reading of low DC current, it is essential to connect the red cable to the positive input of the multimeter and the black cable to the negative input. The battery voltage measurement was determined by carefully holding it for a duration of 5 to 7 seconds. Once the experiment began, the battery voltage was diligently checked and recorded every hour. After the test concluded, we carefully filtered the precipitate that had formed in the salt water using a vacuum filter. It was then subjected to a drying process at a temperature of 100 °C for a period of 24 hours, in order to ensure its readiness for analysis. To perform the chemical analysis of the precipitate, a Shimadzu XRF−1700 model X-ray fluorescence spectrometer (XRF) was utilized. In addition, the Rigaku UltimaIV model X-ray diffraction (XRD) was used to perform the mineralogical analysis of precipitates. The XRD data collection took 10 minutes, using a scanning range of 10 to 80 ° and a size step of 0.02°.

3. Results and Discussion

3.1. Theoretical Background for Discharging Process Using Iron Bed

A substantial amount of metal conducts the electric current, facilitating the wide dispersion of battery discharge in the salt solution. The iron has a standard electrode potential of −0.447V [21, 22] allowing for the creation of an active electric cell in the electrolyte solution. The rapid depletion of battery voltage occurs in iron due to its high electrical resistance, resulting in the conversion of energy into heat. Additionally, it should be highlighted that iron is both affordable and widely

available. During the discharge process, a multitude of electrochemical and electrical processes occur simultaneously. This includes the electrolysis of water, the corrosion of iron, the chlorination of iron, and the generation of sparks from electrical short circuits. Figure 2 provides a visual depiction of this concept, presented in a schematic form for easy understanding. When an electrolyte solution is introduced, the iron undergoes a process where it relinquishes its electrons, consequently leading to the creation of iron ions, such as $Fe \leftrightarrow Fe^{2+}/Fe^{3+}$. Iron from the battery will immediately conduct current to the electrolyte, completing the circuit. The reaction between Fe^{2+} and Cl^-, produced through the decomposition of salt ($NaCl \rightarrow Na^+ + Cl^-$), results in the formation of iron chloride ($FeCl_2$), which then precipitates onto the surface of the iron part. Moreover, the presence of Fe^{2+} results in the formation of $(OH)^-$ through water decomposition, leading to the occurrence of corrosion. When the battery is being discharged, the corrosion products float to the solution's surface, and after the battery is fully discharged, the iron rusts settle down to the bottom of the solution. Observing this phenomenon allows us to determine the progress of battery discharge. In addition, due to the process of electrolysis of water, hydrogen gas is produced at the negative pole of the battery following reaction of $H^+ + 2e^- \rightarrow H_2$. This gas then permeates through the solution and eventually gets removed from it. The gas enters the solution, spreads throughout, and eventually disappears. Additionally, the absence of hydrogen gas being produced was another clear sign that the battery had completely discharged. The phenomenon of stopping the generation of hydrogen gas also indicated that the battery was fully discharged. While using the iron powder, a small fragment managed to slip through the gap between the battery's positive pole, resulting in a short circuit between the steel shell and the cap. As a result, a small portion of iron powder became heated, leading to the ignition of a spark. It was at that particular spot where the insulating plastic gasket, which separates the steel shell and the steel cap, had melted and resulted in a puncture. As the battery electrolyte entered the gap, it dissolved into a solution, which then made its way into the battery.
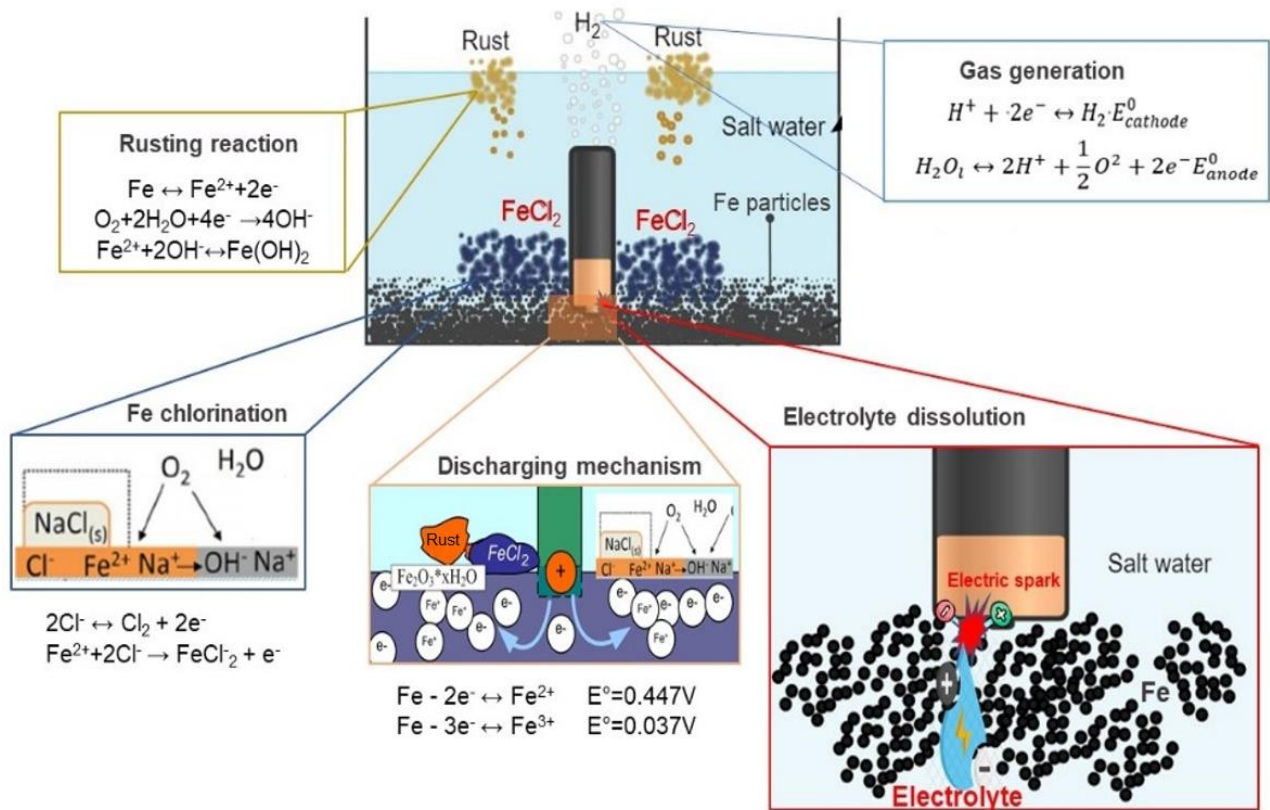
Figure 2.
Schematic diagram of battery discharge using iron bed in salt water.

Several studies, such as Fang, et al. [11]; Shaw-Stewart, et al. [23]; Xiao, et al. [18] and Tennakone [24] have indicated that when a battery is discharged in saltwater, electrochemical reactions occur in an electrolyte circuit. The battery's voltage drop occurs due to the process of water electrolysis, which in turn produces hydrogen gas, as indicated by research findings. The formation of hydrogen bubbles at the negative pole serves as an indication of this phenomenon. Applying a voltage higher than 1.23V triggers an electrochemical process known as water electrolysis, which disassociates water molecules. The occurrence of electrochemical reactions is indicated by Equations 1 to 3, which provide support for both the anode and cathode.

Anode:
$$2H_2O - 4e^- \leftrightarrow O_2(g) + 4H^+ \qquad E^\ominus = 1.23V \qquad (1)$$
Cathode:
$$2H^+ + 2e^- \leftrightarrow H_2(g) \qquad E^\ominus = 0V \qquad (2)$$
Total reaction:

$$2H_2O(l) \leftrightarrow 2H_2(g) + O_2(g) \qquad E^{\ominus} = -1.23V \qquad (3)$$
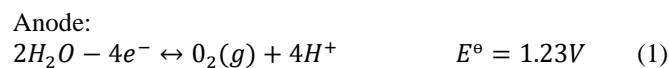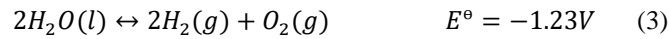
In an aqueous solution, Eh-pH diagrams serve as a tool to illustrate the thermodynamic stability areas of different species. Both pH and electrochemical potential (Eh) scales determine the areas of stability. Figure 3 provides a visual representation of the inverse relationship between Eh and pH in the Fe-Na-Cl system at room temperature, indicating that higher pH values are indicative of lower Eh values. The green dotted lines on the diagrams represent both the upper and lower stability limits of water. The pH level of the solution was found to be 9.75 when the salt water concentration was at 10 wt.%, however, it significantly increased to 10.63 when the concentration was increased to 30 wt.%. When the pH level is between the range of 9 to 11, water dissociation can take place below 1.0V, resulting in a positive increase in battery voltage discharge. Additionally, at range of 9 to 11 pH, the predominant oxidation state of iron is Fe^{2+}. The process in this solution involves the oxidation of Fe^{2+} ions through a series of steps. These steps include the transformation of Fe^{2+} to $FeO \cdot OH$, then to Fe_3O_4, and finally to $Fe(OH)_2$. It is important to note that these steps occur in order to decrease the electrochemical potential. From the discharge phase results, it can be concluded that iron is situated in the oxidation region of Fe_3O_4, thus confirming its presence. While NaCl undergoes decomposition, Na^+ and $Cl(g)$ are formed simultaneously, and both of these substances eventually achieve a state of stability.
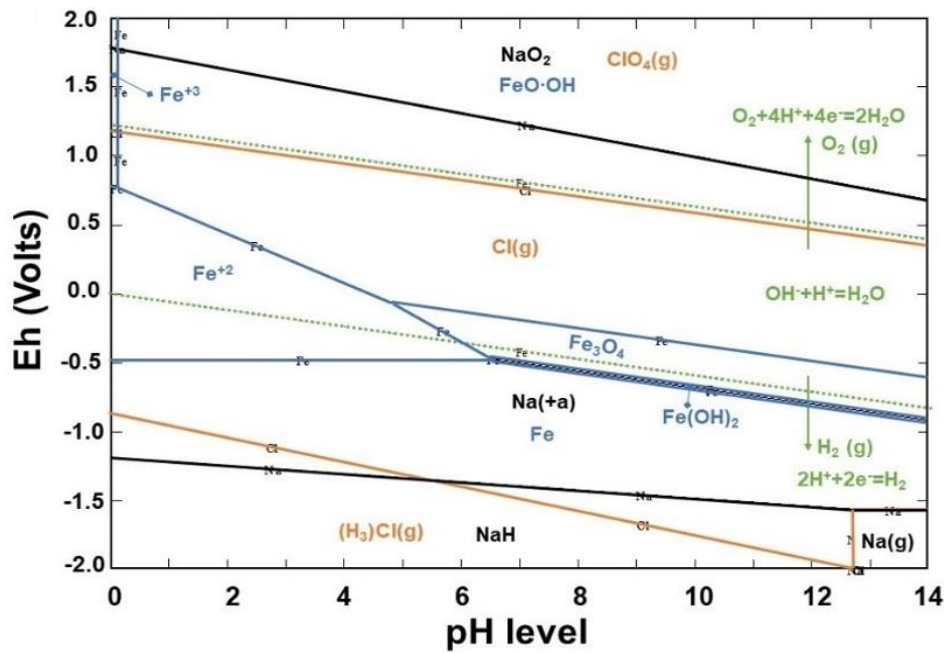
Figure 3.
Eh-pH-diagram for the Fe-Na-Cl systems at 25 °C by HSC−6.2 chemistry.

Apart from the water splitting reaction, the discharge process encompassed two other reactions, specifically the corrosion reaction of iron and the decomposition reaction of salt. A crucial aspect of the electrochemical reaction was the role played by settled iron powder, which was composed entirely of pure iron. The reactions listed below from (4) to (10) represent the redox reactions of elements, which occur at both the anode and the cathode of the battery [25-27]. Oxidation occurs in metals when they are exposed to the oxygen released during the process of water splitting. Furthermore, the oxides produced from this reaction will precipitate and settle at the beaker's base, as shown in Equation 11, 13. Due to the process of salt decomposition, iron underwent a reaction with chlorine as represented by Equation 12, resulting in the formation of iron chlorides.

Anodic half reaction

$$Fe - 2e^- \leftrightarrow Fe2^+ \qquad\qquad E^{\ominus} = 0.47V \qquad (4)$$
$$Fe - 3e^- \leftrightarrow Fe3^+ \qquad\qquad E^{\ominus} = 0.037V \qquad (5)$$
$$2Cl^- - 2e^- \leftrightarrow Cl_2(g) \qquad\qquad E^{\ominus} = -1.35V \qquad (6)$$
$$Na - e^- \leftrightarrow Na^+ \qquad\qquad E^{\ominus} = -2.71V \qquad (7)$$

Cathodic half reaction

$$2H_2O + O_2 + 4e^- \leftrightarrow 4OH^- \qquad\qquad E^{\ominus} = 0.82V \qquad (8)$$
$$Fe^{2+} + 2e^- \leftrightarrow Fe \qquad\qquad E^{\ominus} = -0.47V \qquad (9)$$
$$Fe^{3+} + e^- \leftrightarrow Fe^{2+} \qquad\qquad E^{\ominus} = 0.77V \qquad (10)$$

Chemical reaction

$$Fe^{2+} + OH^- \rightarrow Fe(OH) \qquad\qquad (11)$$
$$Fe + Cl_2 = FeCl_2 \qquad\qquad (12)$$
$$Fe^{2+} + 2H_2O + 2e^- \leftrightarrow FeO + 2H^+ \qquad\qquad (13)$$
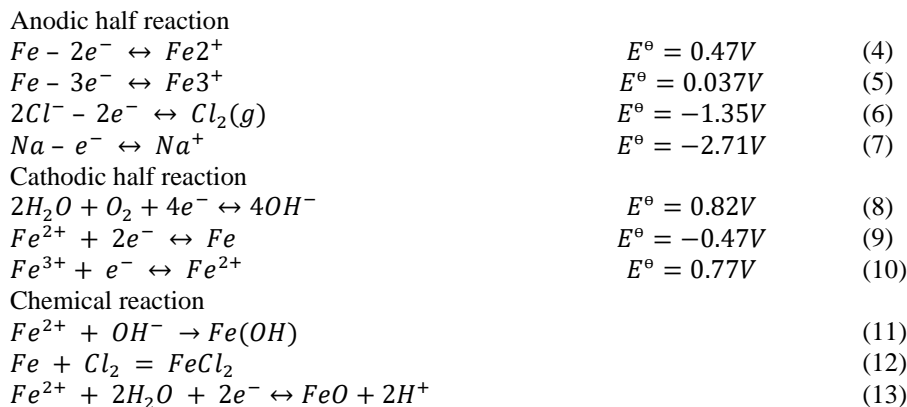
3.2. Battery Discharge in Salt Water with Iron Powder

Figure 4 shows the relationship between time and the rate of battery discharge, demonstrating the curve. The drop in battery voltage can be observed in three distinct stages, each indicated by a dashed black line. The stages of this process consist of constant voltage, bulk voltage drop, and low voltage drop. The battery goes through a constant voltage stage during the discharge process, supplying energy until its capacity depletes and its loses its ability to hold a voltage. After all of the stored energy has been depleted, the battery experiences a rapid decrease in residual voltage during the voltage drop stage. The low voltage stage is the final step in the battery's discharge cycle, as the decreased residual voltage greatly reduces its capacity to support chemical reactions in the electrolyte. At regular intervals of one hour, the battery voltage was measured throughout the entire duration of the battery discharge test. Throughout the first 4 hours of the test, the battery voltage in 10 wt.% salt waters showed no significant changes, but it then started to slowly decrease, reaching 3.5V at the 5-hour mark and eventually dropping to 3.2V after 6 hours. Following an additional hour, the voltage decreased to 1.2V, and subsequently, after a total of 8 hours, it further dropped to 0.2V. It took a total of 10 hours for the voltage to drop down to 0.01V. With the gradual increase in the concentration of the salt water, the discharge rate of the battery started to accelerate. After a constant voltage stage lasting 3 hours, the battery discharged rapidly in the 15 wt.% solution. Subsequently, the voltage dropped to 0.08V, signifying complete discharge, after 8 hours. However, when battery discharge was carried out in solutions of 20 wt.% and 25 wt.%, the intensity was notably higher. The experiment results revealed that the battery discharge conducted in a 20 wt.% salt solution stood out as the most effective among all the other tests performed. The constant voltage stage lasted for 2 hours, but then the battery voltage started to decline, eventually reaching a mere 0.05V after 5 hours. On the other hand, it was observed that the rate of battery discharge is slower in the 30 wt.% salt solution.
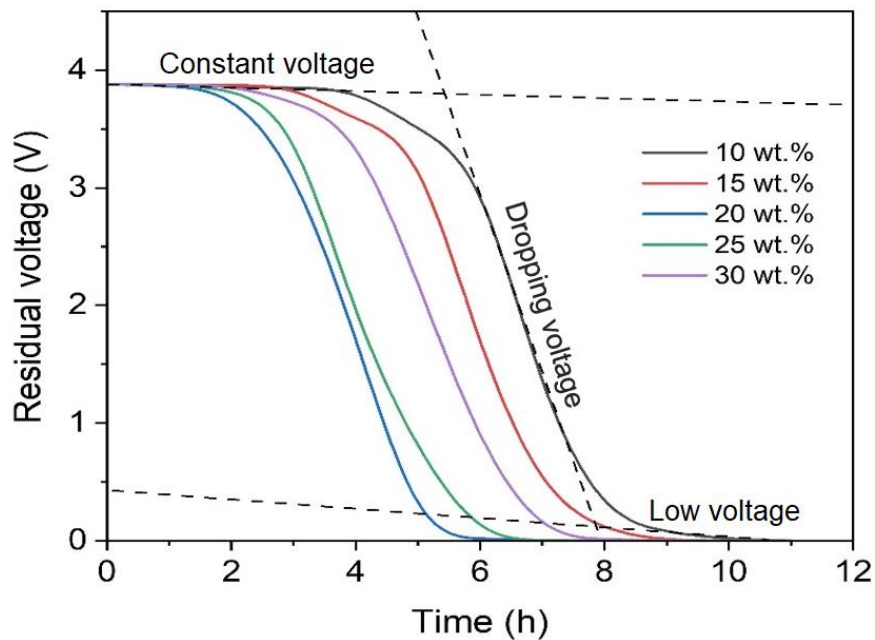
Figure 4.
Relationship between the discharge rate of battery and the concentration of salt water with iron powder.

The assessment of battery discharge efficiency is based on the percentage of residual voltage and voltage drop. The battery's residual voltage percentage (E_t) was determined by calculating the difference between the residual voltage after the discharge test and the initial voltage, as described in Equation 14. In addition to that, the percentage of voltage drop (E_r) was calculated using Equation 15 as referenced in Torabian, et al. [13].

$$E_t = \left(\frac{V_t}{V_0}\right) * 100\% \qquad (14)$$

$$E_r = \left(1 - \frac{V_t}{V_0}\right) * 100\% \qquad (15)$$

Where; V_t is the residual voltage at final time t, and V_o is the initial voltage.

The discharge test results, which were conducted based on the varying concentration of salt water, were subsequently compared with the results obtained after a duration of 6 hours. The battery discharge test, which involved submerging it in both 20 wt.% and 25 wt.% salt water, was successfully completed within 6 hours. Figure 5 provides a comparison between the percentage of residual voltage and the percentage of voltage drop of the battery when discharged using different concentrations of salt water. The batteries experienced a significant drop in voltage, reaching 99.6% and 99.4% in 20 wt.% and 25 wt.% salt water, respectively. This drop in voltage suggests that a complete discharge of the batteries occurred. The 10 wt.% solution showed a minimal voltage drop of 17%, leaving behind a substantial residual voltage of 82.5%. The 15 wt.% solution produced a voltage drop of nearly 59%, indicating a significant enhancement in battery discharge. However, when using a 30 wt.% solution, it has been found that the voltage drop is roughly 80%, providing further evidence that the discharge rate is slower compared to 20 and 25 wt.%.
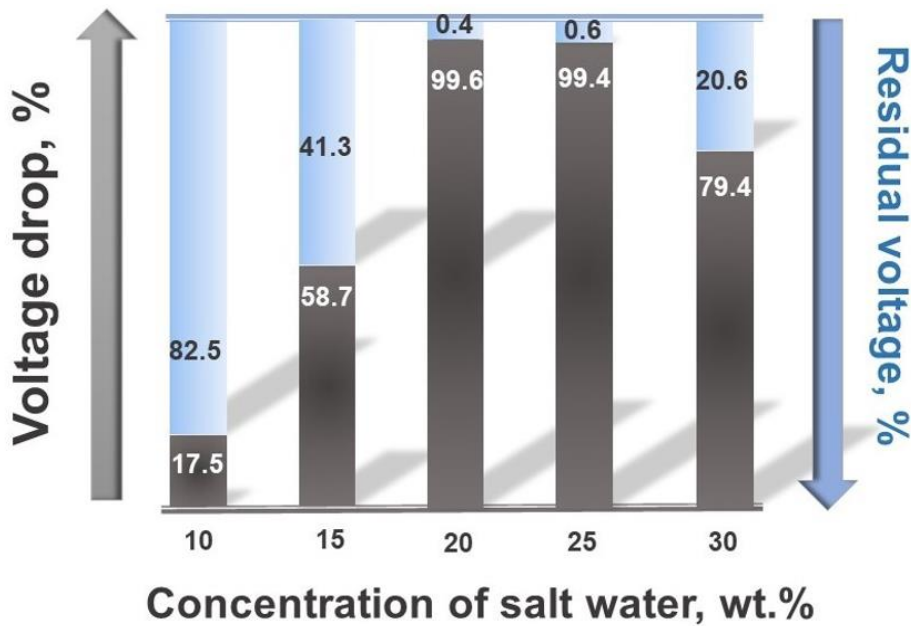
Figure 5.
Battery discharge efficiency depending on concentrate in salt water with iron bed.

The effect of temperature on the battery discharge rate was investigated through a series of tests. The tests were carried out across a temperature range starting from 25 °C and reaching up to 65 °C. Due to the proven effectiveness of the 20 wt.% solution's discharge rate, it was decided to use this concentration in the subsequent experiment. Taking into account the proven effectiveness of the 20 wt.% solution's discharge rate, it was concluded that this concentration would be employed in the subsequent experiment. Figure 6 illustrates the relationship between temperature and discharge rate. The test results indicate that solutions at temperatures ranging from 25 to 35 °C exhibit similar discharge rates, whereas solutions at temperatures between 45 and 65 °C also display comparable discharge rates. The dashed black line on the graph represents the range of these temperatures, and it is worth noting that above 45 °C, there is a slight increase in the discharge rate. The voltage noticeably drops below 0.1V within 5 hours of battery discharge, especially in temperatures exceeding 45 °C. Conversely, the tests taken at 25 °C and 35 °C revealed a voltage of approximately 0.6V. The battery's discharge rate was found to be slightly dependent on temperature, suggesting that temperature has little impact on the battery's discharge.
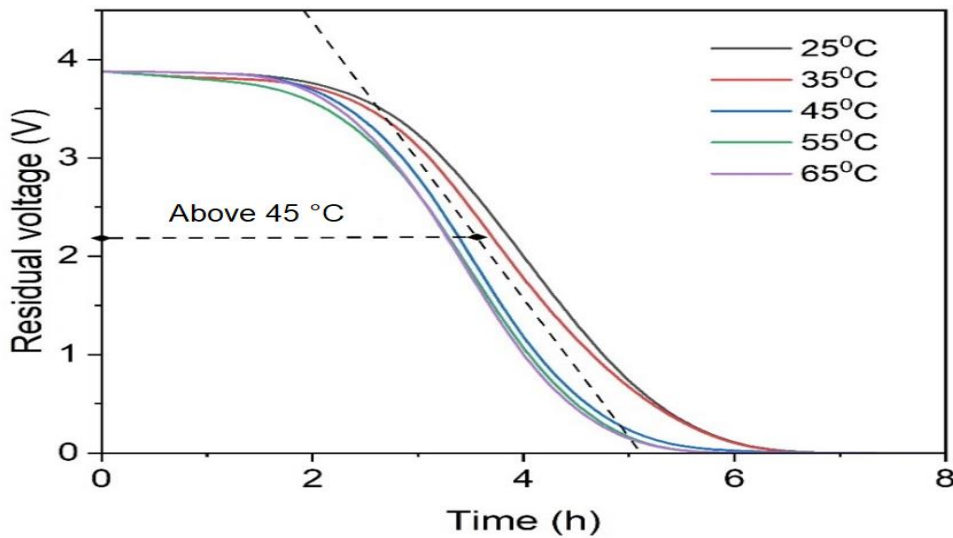
Figure 6.
Relationship between the discharge rate of battery and the temperature of salt water.

The test compared the discharge efficiency in a 20 wt.% salt solution at different temperatures, and the results were then compared to those obtained after 5 hours (Figure 7). Tests conducted at both 25 °C and 35 °C determined an average battery discharge efficiency of 85% with a residual voltage of 15%. However, during the test conducted at a temperature of 45 °C, it was observed that the battery voltage dropped 97%. Furthermore, the discharges conducted at temperatures of 55 and 65 °C, the voltage drop was recorded as 99.5% in each case.
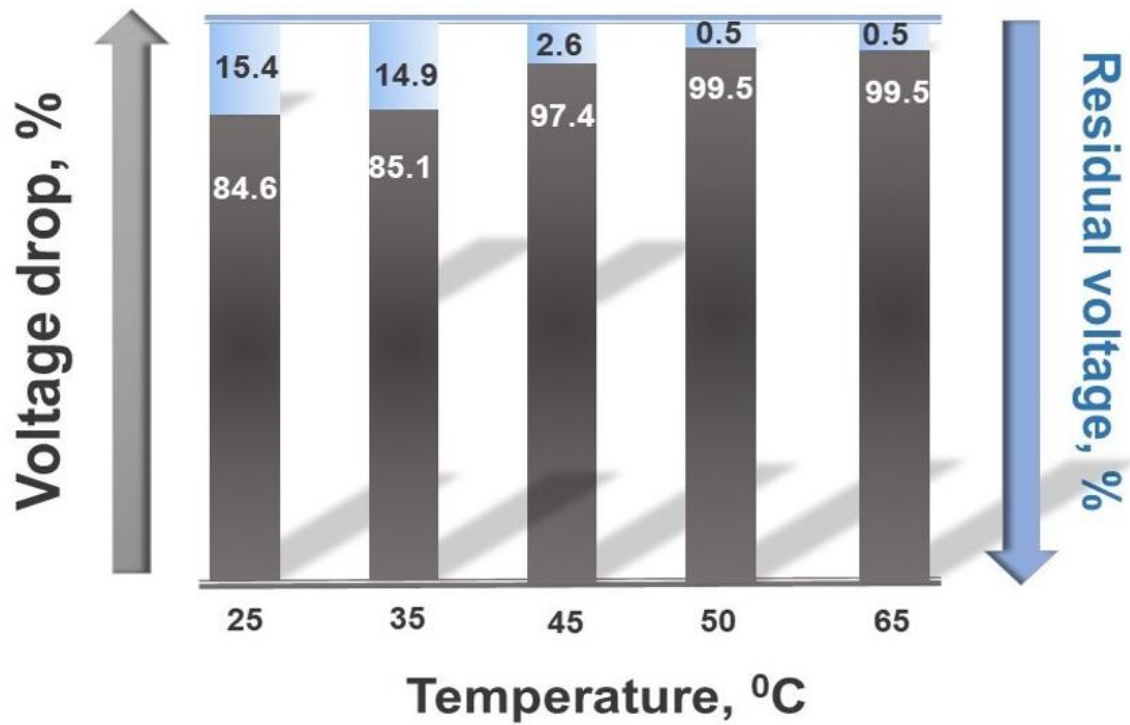
Figure 7.
Battery discharge efficiency in saltwater with iron bed depends on temperature.

Figure 8 shows the discharge process of battery in 20 wt.% salt water, showcasing both the starting and ending states. The figures include the discharged battery, the removed plastic gasket, as well as the anode and cathode foils. At the beginning of the experiment, the solution had a transparent appearance, while small gas bubbles constantly formed and evaporated on the negative pole of the battery (Figure 8a). Once the test concluded, a layer of rust formed on the surface of the solution, creating a reddish-brown film that slowly descended to the bottom (Figure 8b). The steel cap of the battery remained uncorroded even during the discharging process, as shown in Figure 8c. Unfortunately, there was an electrical short circuit, which caused the insulating plastic gasket to melt and subsequently get punctured (Figure 8d). Upon opening the battery, it was observed that the solution had penetrated into both the anode and cathode separators, as shown in Figure 8e and f.
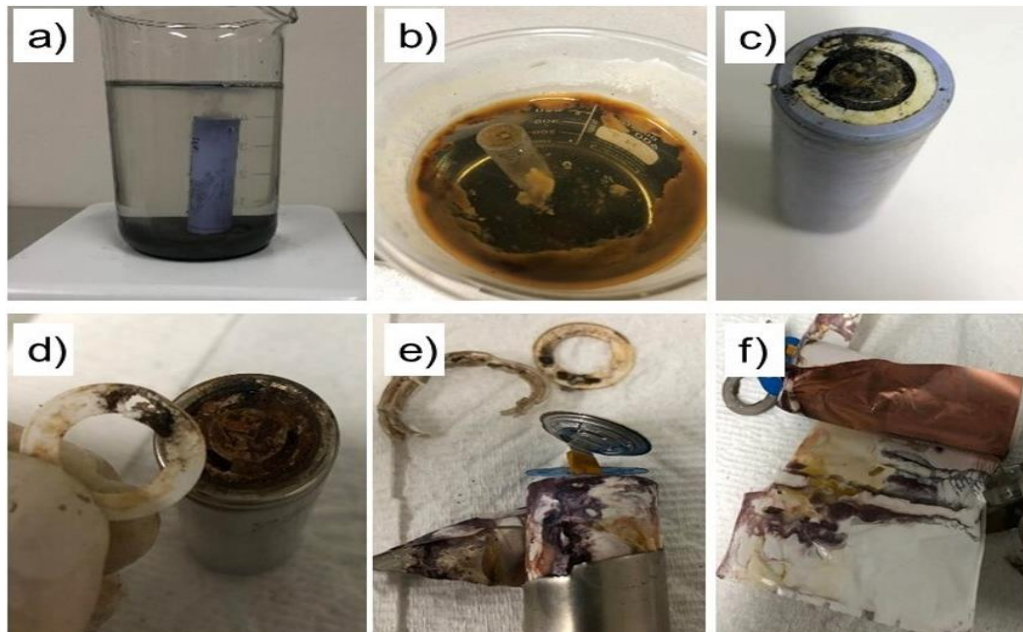
Figure 8.
NCA battery immersed in salt water (a) Before and (b)After discharging using Fe powder, (c) Discharged battery, (d) Insulating plastic gasket damaged by short-circuit spark, (e) Wetted cathode and anode of battery by salt water.

3.3. Chemical Analysis of Precipitate

After completing the discharge tests, a vacuum pump filtered the solution. Following a 3-hour drying process at a temperature of 100 °C, the precipitate that had been filtered underwent XRF and XRD analysis to determine the chemical

compounds present. The precipitates that were formed during the discharge process, which occurred in 20 wt.% salt water at a temperature of 45 °C, were subsequently identified and subjected to analysis. Using XRF analysis, the chemical composition of the precipitate was determined and is presented in Table 2. The analysis revealed that the precipitate primarily consisted of Fe_2O_3, with a measurable amount of Cl at 2.43 wt.%, suggesting the existence of $FeCl_3$. Using the XRF analysis technique, one can exclusively obtain the concentration of elements and have the results conveniently presented in the commonly used oxide form. In addition, it is important to note that XRF analysis is limited in its ability to distinguish between different oxidation states of elements, as it only provides results for the most prominent oxide form. Iron (Fe) can exist in various oxidation states, including FeO, Fe_3O_4, and Fe_2O_3. However, it is important to note that the Fe K-alpha peak is specifically visible in the Fe_2O_3 state [28].

Table 2.
The chemical composition of precipitates by XRF analysis.

Oxides	Fe_2O_3	Cl	Al_2O_3	MnO	Co_2O_3	Cr_2O_3
Wt.%	95.99	2.43	0.79	0.45	0.21	0.12

By using XRD analysis, it becomes possible to conveniently identify the specific oxides and phases that are present in the material. Through XRD analysis, the composition of the precipitate was determined, and this technique also enabled mineralogical analysis, as depicted in Figure 9. The investigation identified the Fe_3O_4 phase as the primary component of the precipitate. The composition of Fe_3O_4 includes Fe^{2+} and Fe^{3+} ions, and it can be expressed as $FeO·Fe_2O_3$ under certain circumstances [29-31]. It is possible that the iron rust $Fe(OH)_2$, which was formed during the discharge process, may have undergone a transformation into the $FeO·Fe_2O_3$ state after it dried. The reason for the undetected $FeCl_3$ phase could be attributed to the low Cl content. However, the detection of a small amount of iron phase suggests the possibility of a samll piece of iron breaking off from the iron flakes. The presence of iron phase in the precipitates suggests that it may have been combined with iron particles originating from powdered iron.
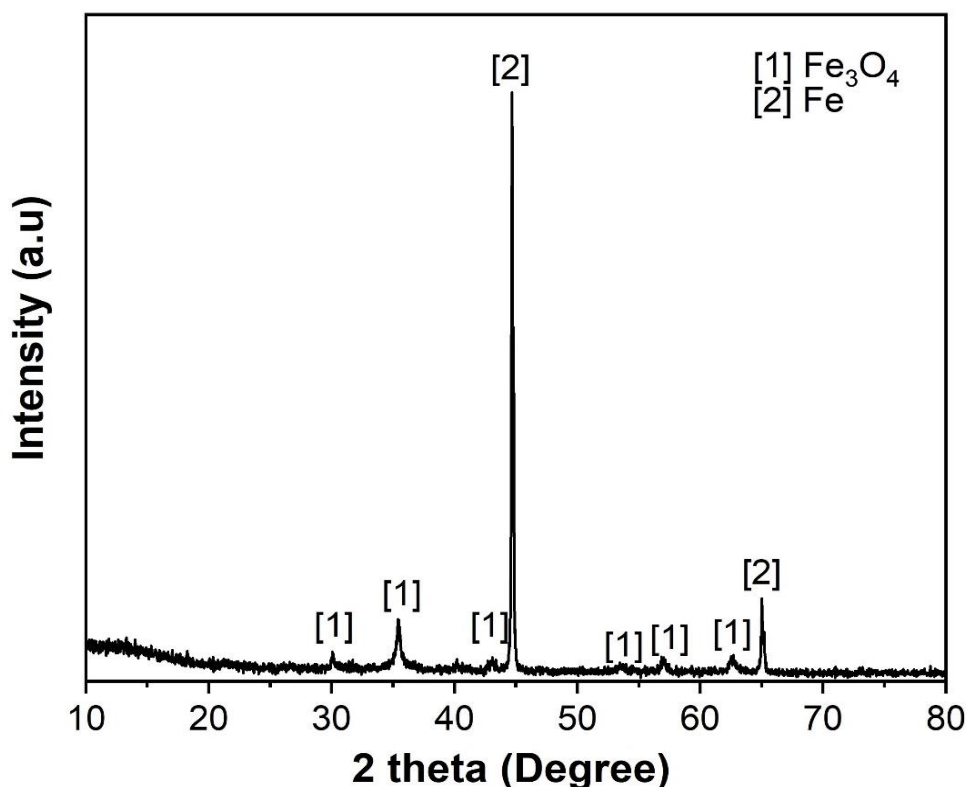
Figure 9.
XRD pattern of precipitate that formed when discharging a battery in salt water with iron bed at temperature of 45 °C.

4. Conclusions

The discharge of the battery in the salt solution with an iron bed can be accelerated by passing the current from the battery through the iron powder bed, thereby creating a large area electrical cell. Placing the battery at the iron powder's positive pole caused the iron parts to receive current, leading to both electrochemical and electrical resistance. Through chemical and mineralogical analysis, it was conclusively determined that the electrochemical reaction of iron resulted in the formation of Fe_3O_4 precipitate on the surface of iron powder. The rate at which the battery discharges can be explained by the thermodynamic stability zone of the Eh−pH diagram for the Fe−Na−Cl system, specifically in relation to the concentration of the salt solution. Increasing the concentration of the salt solution not only elevates the pH level of the solution, but also reduces the electrochemical potential of water electrolysis, thereby enhancing the battery's discharge performance.

Furthermore, according to the diagram, the Fe^{2+} ions have the ability to undergo oxidation by going through a series of steps. These steps include the conversion of Fe^{2+} to $FeO \cdot OH$, followed by the formation of Fe_3O_4, and ultimately leading to the production of $Fe(OH)_2$. Notably, Fe_3O_4 is shown to persist in the oxide state during this entire process. The results obtained from the XRD analysis support this conclusion. The Eh−pH diagram indicates that the discharge efficiency improves as the NaCl content in the solution increases; however, the experiment revealed that the utilization of a 20 wt.% salt solution achieved the highest discharge efficiency, reaching an impressive 99.6% battery discharge within just 6 hours. When the NaCl content in the solution increases, it causes a decrease in the water content and reduces the electrolysis of water, ultimately leading to a decrease in the efficiency of battery discharge. When subjected to a battery discharge test with a 20 wt.% salt solution, the battery discharge rates exhibited a slight increase at temperatures above 45 °C, within the temperature range of 25 to 65 °C. Within a theoretical framework, the research work provides a detailed explanation of the battery discharge method in salt solution with an iron bed. Additionally, it includes experimental data to support the findings. In addition, it is suggested that incorporating the fine Fe_3O_4 oxide, which is generated as a by-product during the battery discharge process, can result in significant economic benefits.

References

[1]   F. Wu, J. Maier, and Y. Yu, "Guidelines and trends for next-generation rechargeable lithium and lithium-ion batteries," *Chemical Society Reviews,* vol. 49, no. 5, pp. 1569-1614, 2020. https://doi.org/10.1039/c7cs00863e

[2]   H. Bajolle, M. Lagadic, and N. Louvet, "The future of lithium-ion batteries: Exploring expert conceptions, market trends, and price scenarios," *Energy Research & Social Science,* vol. 93, p. 102850, 2022. https://doi.org/10.1016/j.erss.2022.102850

[3]   L. Zhou *et al.*, "State estimation models of lithium-ion batteries for battery management system: Status, challenges, and future trends," *Batteries,* vol. 9, no. 2, p. 131, 2023. https://doi.org/10.3390/batteries9020131

[4]   S. Rana, R. Kumar, and R. S. Bharj, "Current trends, challenges, and prospects in material advances for improving the overall safety of lithium-ion battery pack," *Chemical Engineering Journal,* vol. 463, p. 142336, 2023. https://doi.org/10.1016/j.cej.2023.142336

[5]   M. S. Ziegler and J. E. Trancik, "Re-examining rates of lithium-ion battery technology improvement and cost decline," *Energy & Environmental Science,* vol. 14, no. 4, pp. 1635-1651, 2021. https://doi.org/10.1039/d0ee02681f

[6]   K. Itani and A. De Bernardinis, "Review on new-generation batteries technologies: Trends and future directions," *Energies,* vol. 16, no. 22, p. 7530, 2023. https://doi.org/10.3390/en16227530

[7]   F. Tang, T. Jiang, Y. Tan, X. Xu, and Y. Zhou, "Preparation and electrochemical performance of silicon@ graphene aerogel composites for lithium-ion batteries," *Journal of Alloys and Compounds,* vol. 854, p. 157135, 2021. https://doi.org/10.1016/j.jallcom.2020.157135

[8]   R. Patil *et al.*, "Highly stable cycling of silicon-nanographite aerogel-based anode for lithium-ion batteries," *ACS Omega,* vol. 6, no. 10, pp. 6600-6606, 2021. https://doi.org/10.1021/acsomega.0c05214

[9]   L. P. Yao, Q. Zeng, T. Qi, and J. Li, "An environmentally friendly discharge technology to pretreat spent lithium-ion batteries," *Journal of Cleaner Production,* vol. 245, p. 118820, 2020. https://doi.org/10.1016/j.jclepro.2019.118820

[10]   L. Wuschke, H.-G. Jäckel, T. Leißner, and U. A. Peuker, "Crushing of large Li-ion battery cells," *Waste Management,* vol. 85, pp. 317-326, 2019. https://doi.org/10.1016/j.wasman.2018.12.042

[11]   Z. Fang *et al.*, "Comparative study of chemical discharge strategy to pretreat spent lithium-ion batteries for safe, efficient, and environmentally friendly recycling," *Journal of Cleaner Production,* vol. 359, p. 132116, 2022. https://doi.org/10.1016/j.jclepro.2022.132116

[12]   S. Ojanen, M. Lundström, A. Santasalo-Aarnio, and R. Serna-Guerrero, "Challenging the concept of electrochemical discharge using salt solutions for lithium-ion batteries recycling," *Waste Management,* vol. 76, pp. 242-249, 2018. https://doi.org/10.1016/j.wasman.2018.03.045

[13]   M. M. Torabian, M. Jafari, and A. Bazargan, "Discharge of lithium-ion batteries in salt solutions for safer storage, transport, and resource recovery," *Waste Management & Research: The Journal for a Sustainable Circular Economy,* vol. 40, no. 4, pp. 402-409, 2022. https://doi.org/10.1177/0734242x211022658

[14]   H. Wang, G. Qu, J. Yang, S. Zhou, B. Li, and Y. Wei, "An effective and cleaner discharge method of spent lithium batteries," *Journal of Energy Storage,* vol. 54, p. 105383, 2022. https://doi.org/10.1016/j.est.2022.105383

[15]   A. M. Abdalla *et al.*, "Innovative lithium-ion battery recycling: Sustainable process for recovery of critical materials from lithium-ion batteries," *Journal of Energy Storage,* vol. 67, p. 107551, 2023. https://doi.org/10.1016/j.est.2023.107551

[16]   H. Rouhi, E. Karola, R. Serna-Guerrero, and A. Santasalo-Aarnio, "Voltage behavior in lithium-ion batteries after electrochemical discharge and its implications on the safety of recycling processes," *Journal of Energy Storage,* vol. 35, p. 102323, 2021. https://doi.org/10.1016/j.est.2021.102323

[17]   T. Zhang, Y. He, L. Ge, R. Fu, X. Zhang, and Y. Huang, "Characteristics of wet and dry crushing methods in the recycling process of spent lithium-ion batteries," *Journal of Power Sources,* vol. 240, pp. 766-771, 2013. https://doi.org/10.1016/j.jpowsour.2013.05.009

[18]   J. Xiao, J. Guo, L. Zhan, and Z. Xu, "A cleaner approach to the discharge process of spent lithium ion batteries in different solutions," *Journal of Cleaner Production,* vol. 255, p. 120064, 2020. https://doi.org/10.1016/j.jclepro.2020.120064

[19]   Y. Liu, D. Mu, R. Li, Q. Ma, R. Zheng, and C. Dai, "Purification and characterization of reclaimed electrolytes from spent lithium-ion batteries," *The Journal of Physical Chemistry C,* vol. 121, no. 8, pp. 4181-4187, 2017. https://doi.org/10.1021/acs.jpcc.6b12970

[20]   C. Xu, M. Ouyang, L. Lu, X. Liu, S. Wang, and X. Feng, "Preliminary study on the mechanism of lithium ion battery pack under water immersion," *Ecs Transactions,* vol. 77, no. 11, p. 209, 2017. https://doi.org/10.1149/07711.0209ecst

[21]   F. Deng, H. Olvera-Vargas, M. Zhou, S. Qiu, I. Sirés, and E. Brillas, "Critical review on the mechanisms of Fe2+ regeneration in the electro-Fenton process: Fundamentals and boosting strategies," *Chemical Reviews,* vol. 123, no. 8, pp. 4635-4662, 2023. https://doi.org/10.1021/acs.chemrev.2c00684

[22]   J. Jiang and J. Liu, "Iron anode-based aqueous electrochemical energy storage devices: Recent advances and future perspectives," *Interdisciplinary Materials,* vol. 1, no. 1, pp. 116-139, 2022. https://doi.org/10.1002/idm2.12007

[23] J. Shaw-Stewart *et al.*, "Aqueous solution discharge of cylindrical lithium-ion cells," *Sustainable Materials and Technologies,* vol. 22, p. e00110, 2019. https://doi.org/10.1016/j.susmat.2019.e00110

[24] K. Tennakone, "Hydrogen from brine electrolysis: A new approach," *International Journal of Hydrogen Energy,* vol. 14, no. 9, pp. 681-682, 1989. https://doi.org/10.1016/0360-3199(89)90046-3

[25] C. Wang *et al.*, "High-efficiency oxidation of norfloxacin by Fe3+/H2O2 process enhanced via vacuum ultraviolet irradiation: Role of newly formed Fe2+," *Chemosphere,* vol. 286, p. 131964, 2022. https://doi.org/10.1016/j.chemosphere.2021.131964

[26] H. H. P. Quang, N. T. Dinh, T. N. T. Thi, L. T. N. Bao, R. Yuvakkumar, and V.-H. Nguyen, "Fe2+, Fe3+, Co2+ as highly efficient cocatalysts in the homogeneous electro-Fenton process for enhanced treatment of real pharmaceutical wastewater," *Journal of Water Process Engineering,* vol. 46, p. 102635, 2022. https://doi.org/10.1016/j.jwpe.2022.102635

[27] G. Zhu *et al.*, "Rechargeable Na/Cl2 and Li/Cl2 batteries," *Nature,* vol. 596, no. 7873, pp. 525-530, 2021. https://doi.org/10.1038/s41586-021-03757-z

[28] H. Rowe, N. Hughes, and K. Robinson, "The quantification and application of handheld energy-dispersive x-ray fluorescence (ED-XRF) in mudrock chemostratigraphy and geochemistry," *Chemical Geology,* vol. 324, pp. 122-131, 2012. https://doi.org/10.1016/j.chemgeo.2011.12.023

[29] M. H. Hamed, D. N. Mueller, and M. Müller, "Thermal phase design of ultrathin magnetic iron oxide films: From Fe 3 O 4 to γ-Fe 2 O 3 and FeO," *Journal of Materials Chemistry C,* vol. 8, no. 4, pp. 1335-1343, 2020. https://doi.org/10.1039/c9tc05921k

[30] S. Cho, L. Tomas da Rocha, and S.-M. Jung, "Effect of reduction behavior from Fe2O3 to FeO on the formation of metallic Fe in multi-stage reduction," *Ironmaking & Steelmaking: Processes, Products and Applications,* vol. 51, no. 4, pp. 297-306, 2024. https://doi.org/10.1177/03019233241246346

[31] Q. Tang and K. Huang, "Determining the kinetic rate constants of Fe3O4-to-Fe and FeO-to-Fe reduction by H2," *Chemical Engineering Journal,* vol. 434, p. 134771, 2022. https://doi.org/10.1016/j.cej.2022.134771